Surface Coverage Effects on the Formation of Molecular Hydrogen on a Graphite Surface via an Eley−Rideal Mechanism

ARTICLE *in* THE JOURNAL OF PHYSICAL CHEMISTRY A · DECEMBER 2003

Impact Factor: 2.69 · DOI: 10.1021/jp035809n

3 AUTHORS:

Anthony J. H. M. Meijer
The University of Sheffield
97 PUBLICATIONS **1,506** CITATIONS
SEE PROFILE

Andrew J. Fisher
University College London
148 PUBLICATIONS **2,985** CITATIONS
SEE PROFILE

David C Clary
University of Oxford
377 PUBLICATIONS **11,337** CITATIONS
SEE PROFILE

Surface Coverage Effects on the Formation of Molecular Hydrogen on a Graphite Surface via an Eley−Rideal Mechanism

Anthony J. H. M. Meijer*,†

Department of Chemistry, University College London, London WC1H 0AJ, United Kingdom

Andrew J. Fisher*

Department of Physics and Astronomy, University College London, London WC1E 6BT, United Kingdom

David C. Clary*

Department of Physical and Theoretical Chemistry, Oxford University, South Parks Road, Oxford OX1 3QZ, United Kingdom

Received: June 25, 2003; In Final Form: October 3, 2003

The associative desorption of $H_2(v)$ on a graphite(0001) surface via an Eley−Rideal mechanism has been studied using a time-dependent wave packet method. In particular, the importance of a coverage of other light H atoms on the surface was investigated. We find that the H_2 molecules are formed less vibrationally excited than in previous studies with no surface coverage of H atoms. We also find that the presence of other (nonreactive) hydrogen atoms does have an effect on the formation probabilities of $H_2(v)$, especially at low translational energies of the incoming H atom and at resonances.

1. Introduction

The current paper is a continuation of research[1−3] into the formation of H_2 in interstellar space via surface-catalyzed associative desorption. The primary motivation for studying the formation of H_2 and its isotopic analogues on graphite lies in astrophysics. H_2 is the most abundant molecule in interstellar space, which makes its formation an important astrophysical process. H_2 plays an important role as a coolant gas in the collapse of interstellar clouds, leading to the formation of stars. It is also the starting point of many interstellar gas-phase reactions leading ultimately to the formation of complex molecules in space. Note that H itself is the starting point for most gas−surface reactions. It has been studied extensively in recent years, both experimentally[4−13] and theoretically.[1−3,14−28] Other related systems have been studied as well.[29−32]

Despite the importance of H_2, its formation is still poorly understood. It is generally accepted that the dominant reaction mechanism for the formation of H_2 in interstellar space is via surface-catalyzed associative desorption on interstellar dust grains.[33−36] This is the only explanation for the current observed abundances of H_2 in space.[37] In the early universe, other reaction mechanisms, following a radiative association pathway via either H^+ or H^-, would have been important as well, in particular before the formation of dust grains. The precise nature of these dust grains is not known, and they may contain many compounds. However, there is observational evidence from the "extinction hump" at 2200 Å that the dust may at least partially be coated in graphite.[38−41] Therefore, most models include reactions on carbon.[42] In our calculations, we use graphite (0001) as a model for interstellar grains, because graphite is also the material used in current laboratory experiments at UCL on this reaction.[10,11]

Generally speaking, the formation of H_2 on dust grains can occur through two reaction mechanisms, the Langmuir−Hinshelwood mechanism and the Eley−Rideal mechanism.[43] In the Langmuir−Hinshelwood mechanism, both particles involved in the reaction are initially adsorbed on the surface and thermalized to it. Subsequently, these particles move across the surface by tunneling or by diffusion. Upon encountering each other, they react and desorb. The energy released will be partly absorbed by the surface and partly taken away by the product molecule. In the (direct) Eley−Rideal mechanism, only one particle is adsorbed on the surface and thermalized to it. The second particle collides with the first particle without first thermalizing to the surface, forming a molecule which can desorb. Which process is most like the actual process in the interstellar medium is heavily dependent on the actual morphology of the dust grains. However, in general, one can say that the mechanisms described here are extremes and that the actual H_2 formation mechanism is most likely a combination of both. One such combined mechanism is the so-called "hot atom" mechanism, in which the incoming hydrogen atom first moves around on the surface (without thermalizing to it) before encountering the adsorbed "target" hydrogen atom and reacting to form H_2. In a recent reaction kinetics study by Cazaux and Thielens, this process was found to work very efficiently at low temperatures.[44]

These general reaction mechanisms do not imply anything by way of the time the formed H_2 needs to desorb from the surface. The precise nature of the desorption, which is determined by the graphite−H_2 interaction, will have a significant effect on the final H_2 rovibrational distributions. Note there is some experimental evidence based on temperature programmed

* To whom correspondence should be addressed. E-mail: a.meijer@sheffield.ac.uk (A.J.H.M.M.); andrew.fisher@ucl.ac.uk (A.J.F.); david.clary@chem.ox.ac.uk (D.C.C.).

† Present Address: Department of Chemistry, University of Sheffield, Sheffield S3 7HF, United Kingdom.

10.1021/jp035809n CCC: $25.00
Published on Web 11/21/2003

desorption data that the H_2 residence times on the surface may be significant.[8]

In the theoretical study of the formation of H_2, some studies have focused on the Langmuir−Hinshelwood mechanism,[27,28] although most attention has been on the Eley−Rideal reaction mechanism.[1−3,14−21,26] The hot atom mechanism has not been studied yet for this reaction, although some quasiclassical calculations for the formation of H_2 on Ni(100) have been published.[45−48] Both steps of the Eley−Rideal reaction mechanism, i.e., the adsorption of the initial H atoms and the subsequent reaction with another H atom, have been investigated extensively.

With regards to the initial adsorption of hydrogen on dust grains the focus of the discussion has mainly been on the question of whether the initial H is chemisorbed or physisorbed on the surface and whether there is a barrier to chemisorption. Initially, calculations on the adsorption of hydrogen on coronene by Jelloaica et al.,[20] which show a barrier to chemisorption of approximately 0.2 eV and a puckering of the C atom directly underneath the adsorbing hydrogen, were contradicted by calculations done by Farebrother et al. on the adsorption of hydrogen on graphite(0001) using density functional theory with periodic boundary conditions.[1] In the latter calculations, no puckering or barrier was found. Later, Sha and Jackson,[16] Allouche et al.,[26] and Meijer and Fisher[49] found that with a more converged description of the Brillouin zone in the study of H-graphite using periodic DFT one also finds puckering of the underlying C and a barrier to adsorption of the hydrogen atom. Recent experimental results also appear to corroborate the presence of a barrier to chemisorption.[12,13]

The different potentials and different fits to the potentials lead to very different results in the subsequent dynamics calculations. Part of the discrepancy is caused by the treatment of the "unpuckering" of the puckered C atom. Because most approaches do not take this into account dynamically, it has to be dealt with via the potential. Here, two treatments are possible: the C atom can unpucker on the time scale of the H + H−graphite reaction (adiabatic approach)[17,21] or it does not unpucker on the time scale of the H + H−graphite reaction (nonadiabatic approach).[2,15,16] Note that the potential based on the calculations of Farebrother et al.[1] has a similar exothermicity for the formation of H_2, a comparable H−graphite adsorption energy, and a similar decrease of the PES after the interaction region as H_2 leaves the surface as the Sha potential for a slow-moving C. Therefore, the results obtained on the latter potential can be compared directly to the results of the Farebrother potential. Another source of discrepancies between the different results lies in the different fitting methods and/or model potentials used to obtain a global PES from the ab initio points.

Even so, a number of general conclusions can be drawn from all of these calculations. First, H_2 is formed vibrationally highly excited (e.g., vibrational quantum number $\nu = 0-5$,[2] $\nu = 4-7$,[21] or average vibrational quantum number $\langle\nu\rangle = 6$[16,17]). Second, H_2 is also formed rotationally excited (e.g., rotational quantum number $j = 8-11$,[19] $j \approx 13$,[2] or average rotational quantum number $\langle j\rangle = 5-6$[16]). Third, there is a significant isotope effect in that the precise reaction geometry, H-on-surface vs D-on-surface and incoming H vs incoming D, has a big influence on the final reaction probabilities.[3,12,17] This means that one has to be careful applying state-resolved results obtained for HD to the formation of H_2, because the dynamics for the formation of the two different molecules will be different. This could also have significant implications for laboratory experiments on this reaction, because the formation of HD is often studied as a template for the formation of H_2 for experimental reasons.

When we compare the current theoretical results to the experimental data currently available from the Cosmic Dust experiment at UCL, it has to be noted that no states higher than $\nu = 2$ and $j = 3$ have been measured yet.[11] Moreover, preliminary analysis of the data suggests that less than 50% of the available energy is in the H_2 molecule, when it is detected. Additionally, evidence of the barrier of 0.2 eV (or approximately 2300 K) toward adsorption of H on graphite, which was predicted by DFT calculations, has now also been found experimentally.[13] A barrier of this height would make it almost impossible for hydrogen to adsorb on graphite under interstellar conditions or under the conditions in the UCL cosmic dust experiment,[10] although physisorption is of course still possible. In that case, however, one would expect there to be little interaction between the H atoms and the surface as well as between the formed H_2 and the surface. This would mean that approximately 4.7 eV has to be accommodated by the H_2 formed, contradicting the available experimental data. One possible explanation for the discrepancies between calculation and experiment is that in the experiment relatively high flux conditions (compared to the interstellar medium) are used and that in the experiment graphite is used, which is not a single crystal and which will undoubtedly have many defects. This may mean that there could be other H atoms on the surface, which might be able to siphon energy away from the formed H_2 molecule, leading to a molecule with less internal energy detected than might be expected based on the calculations.

The significant rovibrational excitation predicted by theory should make it easy to observe highly excited H_2 in interstellar space via features in the $1-5$ μm spectral range. Attempts so far, however, have been unsuccessful.[22] However, if the H_2 molecule leaves the surface with much less internal excitation than currently predicted by theory, then that may also explain the nondetection of highly excited H_2 in interstellar space. In that case, the features in the $1-5$ μm range, which would be indicative of highly excited H_2 may be so weak that they fall below the detection limit of the telescope used in the observations. An additional source of discrepancy between the calculations and the astronomical observations is our poor knowledge of the composition and morphology of cosmic dust grains. These grains will have significant contamination with elements other than carbon and will not be highly crystalline. Both factors will obviously significantly impact the reaction dynamics for the formation of H_2.

In this paper, we have set out to investigate the role that other (nonreactive) H atoms may play in the outcome of the reaction. To study this systematically, we have placed a uniform monolayer of H atoms on top of a crystalline graphite surface. In wave packet calculations, we then let an H atom collide with a designated H atom on this modified graphite surface to H_2 via the Eley−Rideal reaction mechanism. Only zero impact parameter collisions are considered, and only one of the nonreactive H atoms is allowed to vibrate. The potential for this reaction was obtained from plane wave density functional theory calculations. For more details, we refer to section 2.

This article is setup as follows. Section 2 describes the theory, and section 3 describes computational methods used. Section 4 discusses the results, and section 5 gives the final conclusions.

2. Theory

2.1. Coordinate System, Model System, and Basis Sets. We start by introducing some notation. The incident H atom

has Cartesian coordinates $\mathbf{x}_i = (x_i, y_i, z_i)$, whereas those of the target H atom are given as $\mathbf{x}_t = (x_t, y_t, z_t)$. We find it more convenient to use Jacobi coordinates in our calculations. Thus, we use the relative position vector $\mathbf{r} = \mathbf{x}_t - \mathbf{x}_i$ and the center-of-mass position vector $\mathbf{X} = (m_i\mathbf{x}_i + m_t\mathbf{x}_t)/(m_i + m_t)$, where m_i and m_t are the masses of the incident and target atoms, respectively. $\mathbf{r}$ is most conveniently expressed in polar coordinates $\mathbf{r} = (r, \vartheta, \varphi)$, where r is the length of $\mathbf{r}$ and ϑ and φ are the polar and azimuthal angles, respectively. $\mathbf{X}$ is used in Cartesian coordinates $\mathbf{X} = (X, Y, Z)$, where X, Y, and Z indicate the position of the center-of-mass of the molecule above the surface. As well as the two reacting atoms, we include a nonreactive spectator H atom into some of our calculations. This has the Cartesian coordinates $\mathbf{x}_s = (x_s, y_s, z_s)$. All other atoms on the surface are assumed to be frozen in their equilibrium configuration. We assume that there is a full monolayer coverage of hydrogen on the surface initially, i.e., two hydrogens per unit cell.

To make our calculations tractable, we make the following assumptions. We assume that the surface is fixed, i.e., phonons are excluded from our calculations. This should be a reasonable approximation for the dynamics of this system, because of the mass difference between H and C. Also, Ruttigliano and coworkers have shown[19] in a mixed classical-quantum calculation in which the phonons were included (classically) that energy transfer to the solid is small. Also, as mentioned above, all hydrogens on the surface, except for the spectator and target atoms are frozen in their minimum energy positions. We also assume that the spectator hydrogen can only move in the z direction. Moreover, we assume that there are only perpendicular zero impact parameter collisions. This will allow us to determine a lower limit for the influence of the nonreactive hydrogens on the reaction probability. This does mean that we do not assume the surface to be flat as in previous calculations.[2,3]

The basis functions in Z, r, and z_s, as in ref 2, are "wrapped" sinc-DVR (discrete variable representation) functions.[50−53]

2.2. Potential. As in our earlier calculations,[2,3] we have used a LEPS (London−Eyring−Polyani−Sato) potential, adapted for use with surfaces.[54] This potential is given as

$$V(z_i, z_t, r) = U_{as}(z_i) + U_{as}(z_t) + U_{aa}(r) - \{[Q_{as}(z_i) + Q_{as}(z_t)]^2 + Q_{aa}{}^2(r) - Q_{aa}(r)[Q_{as}(z_i) + Q_{as}(z_t)]\}^{1/2} \quad (1)$$

where aa indicates an atom−atom interaction and as an atom−surface interaction. The terms $U_\beta(d)$ and $Q_\beta(d)$ with $\beta \in \{\text{aa}, \text{as}\}$ and $d \in \{z_i, z_t, r\}$ are defined as

$$U_\beta(d) = \frac{D_\beta}{4(1+\Delta_\beta)}[(3+\Delta_\beta)e^{-2\alpha_\beta(d-d_\beta)} - (2+6\Delta_\beta)f_\beta(d)e^{-\alpha_\beta(d-d_\beta)}] \quad (2)$$

$$Q_\beta(d) = \frac{D_\beta}{4(1+\Delta_\beta)}[(1+3\Delta_\beta)e^{-2\alpha_\beta(d-d_\beta)} - (6+2\Delta_\beta)f_\beta(d)e^{-\alpha_\beta(d-d_\beta)}] \quad (3)$$

In our earlier papers $f_\beta(d)$ equalled 1. Those potentials will be designated standard LEPS (SLEPS). The $f_\beta(d)$ term is defined as[55]

$$f_\beta(d) = \exp\left[\frac{\alpha'_\beta(d-d_\beta)}{1+e^{-\alpha''_\beta\alpha_\beta(d-d'_\beta)}}\right] \quad (4)$$

It was found in fitting DFT calculations for the Ni + H_2 system that including the $f_\beta(d)$ term in the calculations improved the long-range behavior of the potentials.[45,46,55] These potentials will be called modified LEPS (MLEPS). Note that there is a slight difference in our use of the $f_\beta(d)$ term compared to the approach taken by, e.g., Sha, Jackson and Lemoine.[17] In their calculations, $f_\beta(d)$ is always one for the incident atom and not necessarily one for the target atom, which introduces a asymmetry in the potential for exchange of the two hydrogen atoms. Therefore, we have chosen to treat all hydrogens equal, which means that there is one $f_\beta(d)$ for all atom−surface interactions. This ensures that in an exchange-type reaction, where effectively at the end of the reaction the incoming and target atoms have exchanged places, the potential at the beginning and at the end of the calculation are identical.

Starting from the LEPS potential defined above, we build the potential for the entire covered graphite surface. We do this by viewing $V(z_i, z_t, r)$ as the interaction potential between hydrogen atoms k and l, writing as $V_{kl}(z_k, z_l, r_{kl})$. The interaction potential $\mathcal{V}'$ for the entire system is then build up from these pair-potentials as

$$\mathcal{V}'(z_1, ..., z_N; r_{12}, ..., r_{N-1N}) = \sum_{k>l}^{N}\sum_{l=1}^{N} V_{kl}(z_l, z_k, r_{kl}) - (N-2)\sum_{k=1}^{N} U_{as}(z_k) + (N-2)\sum_{k=1}^{N}|Q_{as}(z_k)| \quad (5)$$

where N is the total number of atoms in the hydrogen layer. The last two terms in eq 5 are included to avoid problems with counting interactions more than once. This term has this specific form, because each atom is involved in $(N-1)$ pairs. Therefore, $(N-2)$ atom−surface interactions must be subtracted to obtain the correct potential. The potential as given in eq 5 shows the correct asymptotic behavior with respect to removal of any of the hydrogens atoms from the surface. It also reverts to the single adsorbed atom potential, if the distances between the H atoms on the surface become very large.

2.3. Hamiltonian, Propagation, Analysis, and Initial States. Our choice of coordinates gives the following Hamiltonian:

$$\hat{H} = \frac{-1}{2m_H}\frac{\partial^2}{\partial z_s^2} - \frac{1}{2\mu_{H_2}}\frac{\partial^2}{\partial r^2} - \frac{1}{2m_{H_2}}\frac{\partial^2}{\partial Z^2} + V(z_s, r, R) \quad (6)$$

where m_H is the mass of the hydrogen atom, μ_{H_2} is the reduced mass of the hydrogen molecule, and m_{H_2} is the mass of the hydrogen molecule. Finally, $V(z_s, r, R)$ is the interaction potential. A pictorial representation of the coordinates is given in Figure 1.

The initial wave function is generated as a function of z_i, z_s, and z_t, the heights of the incident, spectator, and target atoms above the surface, respectively, as

$$\Phi(z_i, z_t, z_s) = \frac{1}{\sqrt[3]{2\pi\beta}}e^{-ik_0z_i}e^{-(z-z_0)2/4\beta}\varphi_0(z_t, z_s) \quad (7)$$

Here, $\varphi_0(z_t, z_s)$ is the lowest eigen state of the two-dimensional vibrational Hamiltonian, which governs the two atoms that are initially in the hydrogen layer. However, the interaction between the target and spectator atoms is very isotropic, which means we can assume that $\varphi_0(z_t, z_s) = v_0(z_t)w_0(z_s)$, where $v_0(z_t)$ and $w_0(z_s)$ are the lowest eigenfunctions of the one-dimensional vibrational Hamiltonians for the target and spectator atoms, respectively. For the propagation, this initial wave function is transformed from the (z_i, z_t, z_s) coordinates to the (Z, r, z_s)

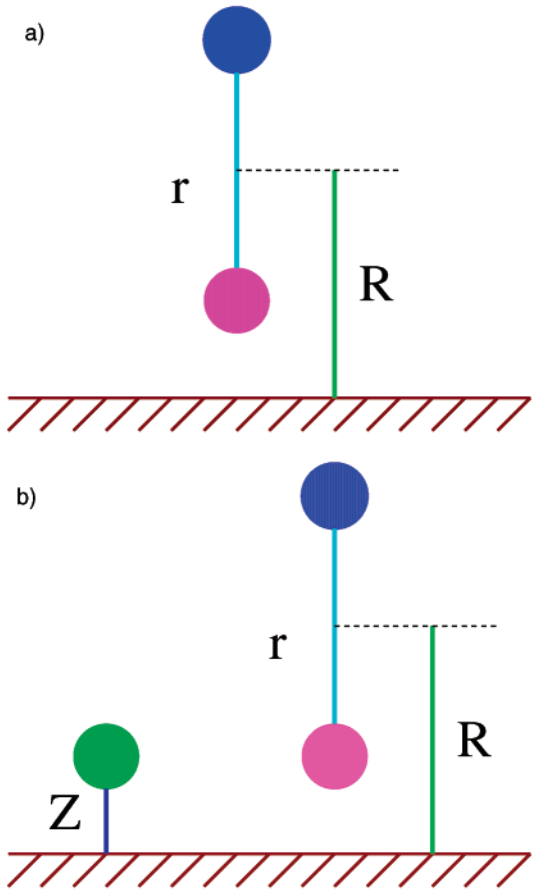

Figure 1. Coordinates included in calculation: (a) 2D calculations and (b) (2+1)D calculations.

coordinates. This requires interpolation of $v_0(z_t)$ and $w_0(z_s)$, which is straightforward, since both are very smooth.[2]

The wave function is propagated in time using the real wave packet method of Gray and Balint-Kurti.[56−59] In this method, reaction probabilities are calculated from only the real part q of the wave packet Ψ. q is propagated in time using a modified Schrödinger equation where $\hat{H}$ is replaced by a function of itself, $f(\hat{H})$. For a judicious choice of $f(\hat{H})$, the propagation is given by a Chebychev recursion relation.[56,58,59] During the propagation, the wave packet is damped at the edges of the grid to avoid unphysical reflections.[60]

The final analysis is performed using a flux-based method.[57,61−63] In this method, the total reaction probability, $P_r(E)$, is calculated from the energy-dependent flux through a surface in the exit channel at $Z_s = 7.9$ Å. The reaction probability as a function of total energy, $P(E)$, is defined as

$$P(E) = \frac{\hbar}{\mu}\mathrm{Im}\,\langle\Psi^+(E)|\hat{F}(Z_s)|\Psi^+(E)\rangle \qquad (8)$$

where μ is the reduced mass of H_2 and $\hat{F}(Z_s)$ is the flux operator for the flux through a surface at Z_s. $\Psi^+(E)$ is the scattering wave function. The state-resolved reaction probability, $P_{v\lambda}(E)$, is simply obtained by introducing the projection operator $\hat{\mathscr{P}}_{v\lambda}$, which is defined as[63]

$$\hat{\mathscr{P}}_{v\lambda} = \frac{1}{P(E)}|v_v(r)w_\lambda(z_s)\rangle\,\langle w_\lambda(z_s)v_v(r)| \qquad (9)$$

which projects $\Psi^+(E)$ onto the vibrational eigenfunctions of the H_2 molecule, which are labeled by v and onto the vibrational eigenfunctions of the bond between the spectator atom and the graphite, which is labeled by λ. Division by $P(E)$ ensures that the state selected reaction probabilities add up to one. The nonreaction probability can be defined in a similar way to $P(E)$, only in this case the surface lies at r_s. The fact that the probabilities always sum to one for a converged calculation is a diagnostic on the quality of the calculation. Note that we plot $P(E_i)$ in section 4, where E_i is the initial translational energy of the incoming H atom.

3. Computational Details

3.1. Potential. *3.1.1. Electronic Structure Calculations.* All electronic structure calculations were performed using density functional theory including gradient corrections, using the Perdew and Wang-91[64] exchange-correlation functional. The program used was VASP 4.4.4.[65−68] All calculations were run on the SGI Origin 2000 at the HiperSpace center at University College London. We used a 3 × 3 × 1 Monkhorst-Pack sampling for the k points. This was sufficient to reproduce the graphite-H interaction potential as calculated by Sha and Jackson,[17] who used more k points in their calculations. The box size in our calculations was 13.92 bohr by 13.92 bohr by 60 bohr (7.37 × 7.37 × 31.75 Å), which is large enough to exclude the interaction of particles with their mirror images. We used the standard "ultrasoft" pseudo potentials, which have plane wave cutoffs of 286.744 eV for C and 349.404 eV for H.

The procedure to calculate the potential energy points was as follows: First we optimized the distance of a complete H layer with respect to a single layer of carbon atoms. The optimum distance was found to be 6.63 bohr (3.51 Å) above the surface with a binding energy of 92 meV of the complete layer to the graphite surface. The energy needed to extract a single H atom from that layer was found to be 2.50 eV. The exothermicity of this potential was found to be 2.05 eV, which is considerably lower than the exothermicity of 2.75 eV for the potential with a single adsorbed H atom, which was used for the calculations in refs 2 and 3.

Subsequently, we generated about 90 potential energy points, mainly concentrating on the entrance and interaction regions of the potential energy surface. If we had used a spline-fit to fit our surface, this would not have been sufficient. However, because we use a simple model potential, this is sufficient. During these calculations all nonreactive atoms were supposed to be in their minimum energy position, apart from the Carbon atom directly beneath the target H atom, whose position was optimized.

3.1.2. Fitting of Model Potential. There are 8 (14) fit parameters for the SLEPS (MLEPS) potential. Of these, three (six) model the C−H interaction, and three (six) model the H−H interaction. The final 2 parameters are the Sato paramters, Δ_β, which model the coupling between the two interactions.

First, we fitted the H−H parameters D_m, α_m, and d_m for the SLEPS potential, and the D_m, α_m, d_m, α'_m, α''_m, and d'_m parameters for the MLEPS potential. This was done by calculating the rovibrational energies of H_2 in a potential generated by a specific set of parameters. These were subsequently optimized against the 320 experimentally observed rovibrational levels,[69,70] using a least-squares fitting algorithm. Because this calculation is quite time-consuming, we first fitted a subset of eigenvalues with random start-up parameters. The best results from this procedure were subsequently used as startup parameters for the complete set. For the least-squares fitting part of our program, we used subroutine E04UNF from the NAG library.[71]

After the calculation of the H−H parameters, we fitted the remaining parameters to the DFT points. As mentioned above,

TABLE 1: Table of Fitting Parameters

parameter	SLEPS		MLEPS	
D_{as}	0.087845	hartree	0.066508	hartree
Δ_{as}	−0.25		−0.314939	
α_{as}	0.70000	$bohr^{-1}$	0.49007	$bohr^{-1}$
d_{as}	6.57	bohr	6.61449	bohr
α'_{as}	0.0		0.40592	$bohr^{-1}$
α''_{as}	0.0		6.68939	$bohr^{-1}$
d'_{as}	0.0		7.50049	bohr
D_{aa}	0.174559	hartree	0.174559	hartree
Δ_{aa}	0.27		0.433609	
α_{aa}	1.045838	$bohr^{-1}$	1.021897	$bohr^{-1}$
d_{aa}	1.40547	bohr	1.411680	bohr
α'_{aa}	0.0		0.206920	$bohr^{-1}$
α''_{aa}	0.0		2.227382	$bohr^{-1}$
d'_{aa}	0.0		3.521245	bohr

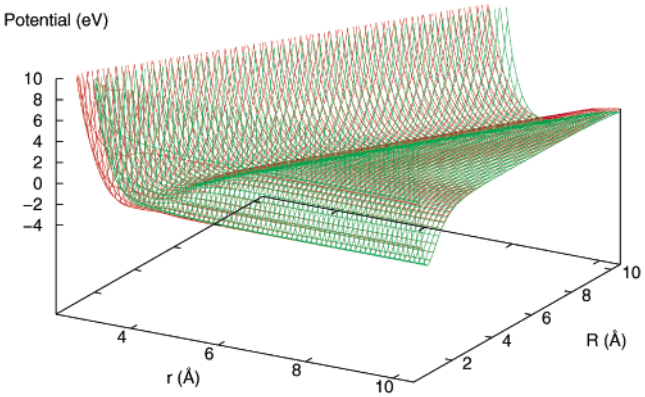

Figure 2. Model potentials: (green) SLEPS fit and (red) MLEPS fit.

these were mainly in the entrance and interaction regions of the PES. We had to scale the DFT points by 4% to get the proper dissociation energy for H_2. The C−H and Sato parameters were optimized by hand to obtain a fit that was as close as possible to the DFT points without introducing artifacts in the potential. This could not be done automatically, since such artifacts were unavoidable in that case, because certain areas were only sparsely populated with electronic structure points.

The resulting parameters for the SLEPS and MLEPS potentials are given in Table 1. The potentials are plotted as a function of r and R at the equilibrium distance of z_s in Figure 2, parts a and b. The MLEPS potential shows better agreement with the DFT points, in particular in the entrance region. This is due to the extra term f_β term in the attractive part of the potential. This gives the fit some extra flexibility to accommodate the almost harmonic potential in which the target atom moves within the H layer.

Finally, we have to point out here that approximations have to be made in the construction of the PES, both in the electronic structure calculations, where, e.g., we had to restrict ourselves to using DFT, which has known problems in describing physisorption interactions, and in the fitting process, where, e.g., we predetermined the form of the interatomic potential. Therefore, this potential can only be considered to give a qualitative rather than a quantitative description of the "real" interaction potential. However, similar approximations were made in earlier potentials, which means that comparison with the earlier results should give meaningful results. Moreover, these calculations should give us a good idea of the influence of the changes in the potential on the dynamics and the subsequent state-resolved reaction probabilities.

3.2. Quantum Dynamics Calculations. We performed two sets of calculations. In the first set of calculations, we only include the r and R coordinates into our calculations. This coordinate system is identical to the one used in the 2D calculations in refs 2 and 3. In the second set of calculations, we also included the z_s coordinate in our calculations. These calculations will be indicated (2+1)D calculations.

To facilitate our calculations, we use the sorting algorithm of Groenenboom and Colbert,[51] as well as the point selection algorithm of Meijer and Goldfield.[62] We performed our calculations on the 48 processor Origin 2000 at the Hiperspace Center at University College London using the DDPHP (doubly distributed parallel $\hat{H}\Psi$) method, recently developed by one of us.[72] The key idea behind this algorithm is to distribute the entire wave packet *twice*, so that each processor in the calculation contains two *different* slices of the wave packet. This means that no communication between the processors is required for all computations. The wave packet only needs to be resynchronized after each $\hat{H}\Psi$ iteration. The result is that the percentage of the wave packet that has to be transferred in each iteration *decreases* with an increasing number of processors. This is in contrast to an algorithm in which the wave packet is only distributed once, because in that case the percentage of the wave packet to be transferred in each iteration actually *increases* with increasing number of processors. The efficient communication characteristics of the DDPHP algorithm combined with an efficient computational layout means that the algorithm scales linearly with an increasing number of processors.[72] Use of the DDPHP algorithm greatly reduced the turn-around time for our calculations.

4. Results

4.1. 2D Calculations. The SLEPS results in this paper will be compared to the results for the single H adsorbed situation, which were published in refs 2 and 3. To aid in the discussion, we have reprinted panel a of Figure 1 in ref 3 as Figure 3c. We will not compare the results for the MLEPS potential with the results from these references, because the functional forms of the LEPS potentials are quite different. We will only compare these MLEPS results to the SLEPS results discussed below.

4.1.1. SLEPS Potential. The 2D results for the SLEPS potential are plotted in Figure 3a. Comparing these results to Figure 3c shows that the change in potential has led to a drop in the vibrational excitation of the product H_2 molecule. We note here that the drop cannot be due to the kinetic energy part of the Hamiltonian used, because the one used here is identical to the one used in ref 2 and 3, even though they describe completely different dynamical systems.

Comparing these results to the earlier results plotted in Figure 3c, it is clear that the change in potential has brought a decrease in the maximum H_2 vibrational quantum number from $\nu = 6$ (channel opens at 1000 K) to $\nu = 4$ (channel opens at 250 K). Also, we find at low energy that the most populated states are $\nu = 2$ and $\nu = 3$, where as before it was $\nu = 3-5$. Another difference is that the current reaction probabilities fluctuate more with increasing translational energy than the earlier results. In Figure 3a, we also find two resonances at 280 and 920 K, comparable to the feature found at 1150 K in Figure 3c. These resonances are most likely excited states of H_2 within the H-layer, although specific assignment should be done by calculating time-independent wave functions, which lies outside the scope of the current work. Between 400 and 600 K, we also see significant changes in the reaction probabilities, in particular a decrease in $\nu = 2$ and an increase in $\nu = 3$, very similar to the resonances found for the formation of HD from adsorbed H in ref 3, although in this case it is not accompanied

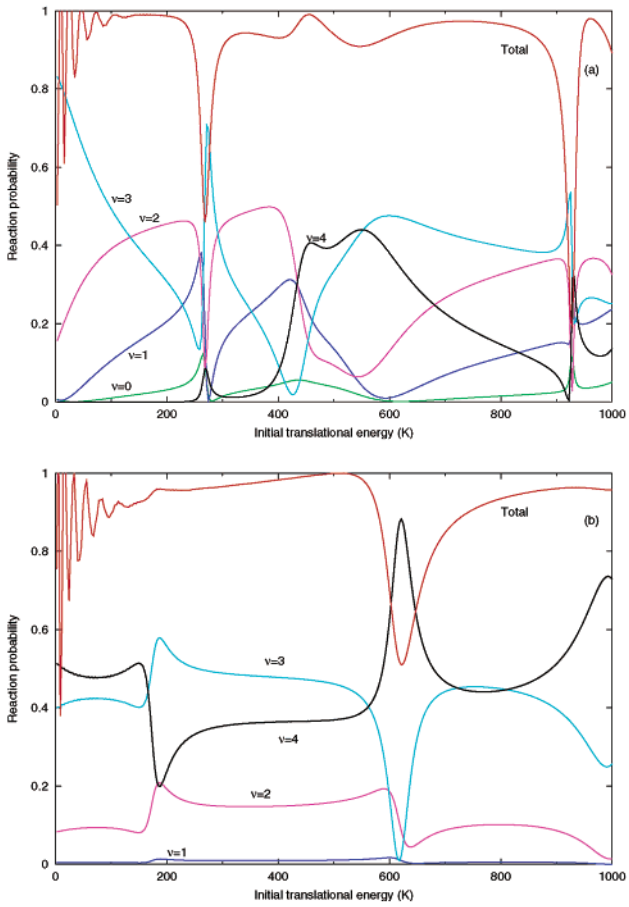

Figure 3. Reaction probabilities as a function of the initial translational energy of the incoming H atom for the 2D calculations: (a) SLEPS potential and (b) MLEPS potential.

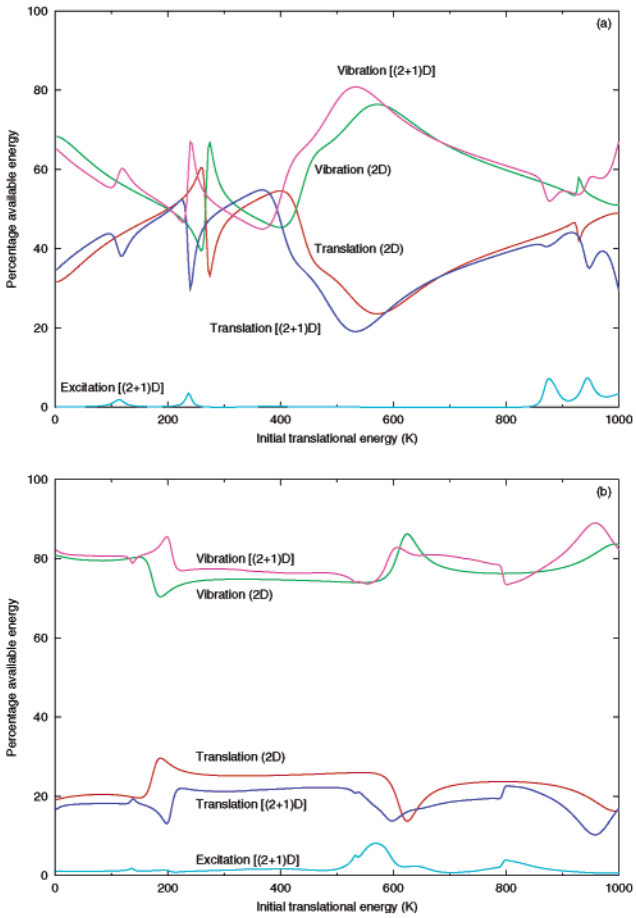

Figure 4. Percentage translational, vibrational, and excitation energy of the total available energy as a function of the initial translational energy of the incoming H atom for the 2D and (2+1)D calculations: (a) SLEPS potential and (b) MLEPS potential.

by a sharp decrease in the total reaction probabilities. If the area between 400 and 600 K is also a (broad) resonance, then it is of a different type than the ones at 280 and 920 K, where changes in the reaction probabilities are much more abrupt.

In Figure 4a, we plotted the average translational energy for the product H_2 molecules as a percentage of the total available energy as a function of the initial translational energy of the incoming H atom. The percentage translational energy varies around 40%, which is similar to the result obtained in ref 2. The main difference with the earlier work is the much wider variation in Figure 4a. The sharp resonances from Figure 3 are clearly still present. Note that we find a much lower percentage translational energy for the H_2 product between 400 and 600 K than anywhere else.

4.1.2. MLEPS Potential. It is clear from comparing part a to part b of Figure 3 that using the MLEPS form of the potential leds to higher vibrational excitation of the product. This has to be due to the wider entrance channel of the MLEPS potential. This leads to a much less tight transition from entrance channel to exit channel. In classical terms, the wider entrance channel leads to a larger portion of phase space becoming accessible, including areas in which the adsorbed H has a relatively large vibrational distance upon entering the interaction region.

Interestingly, the wider entrance channel also makes the dependence of the reaction probabilities on the initial translational energy of the incoming H atom much smoother and less variable. We find two sharp resonances, one at 200 K and one at 600 K. Again, these correspond most likely to excited states of H_2 in the H layer. These resonances are found at lower initial translational energies than in the case of the SLEPS potential, which has to be due to the wider entrance channel in the MLEPS case, which leads to lower excitation energies for the adsorbed H and H_2. We can find no evidence of any features, which might be broad resonances, like the one found for the SLEPS potential between 400 and 600 K.

The higher vibrational excitation of the H_2 product is also evident from the plot of the translational energy as a percentage of the total energy as a function of the initial translational energy, plotted in Figure 4b. Here, we find only 20% translational energy and 80% vibrational energy, compared to 40% and 60%, respectively in Figure 4a. Also, the MLEPS curves are fluctuating less with initial translational energy than in the SLEPS case, which is entirely consistent with the reaction probabilities.

4.2. (2+1)D Calculations. *4.2.1. SLEPS Potential.* In Figure 5a, we plotted the reaction probabilities for the (2+1)D calculations summed over all states of the spectator atom. Comparing these results with the results for the 2D calculations in Figure 3a, we see that the two are broadly similar. The main differences are the suppression of the resonance at 920 K and the emergence of a resonance at 100 K. The broad feature between 400 and 600 K is not affected as much as the resonances. This picture is emphasized if we investigate the state-resolved reaction probabilities, summed over all H_2 states. These are plotted in Figure 6a per state ξ of the spectator atom as a function of initial translational energy. The resonances at 200 K and around 900 K show significant excitation of the spectator atom, whereas the broad feature between 400 and

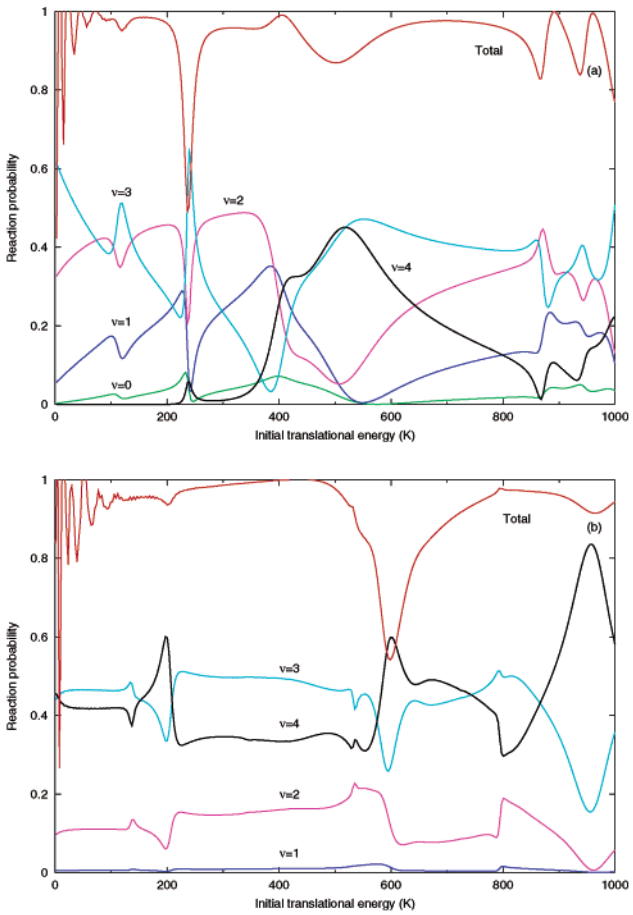

Figure 5. Reaction probabilities summed over all states of the spectator atom for the (2+1)D calculations: (a) SLEPS potential and (b) MLEPS potential.

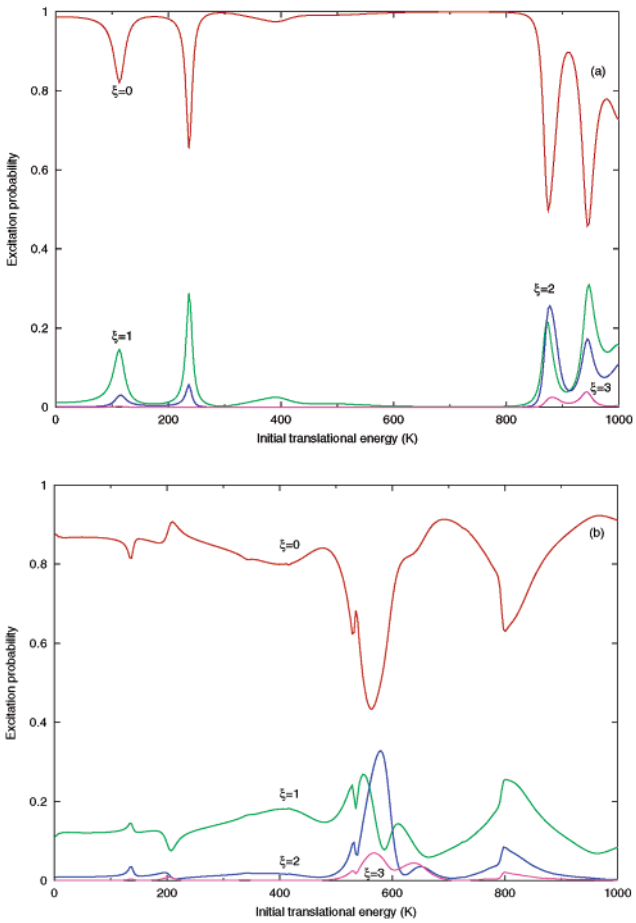

Figure 6. Excitation probabilities for the spectator H atom summed over all H_2 vibrational states as a function of the initial translational energy of the incoming H atom: (a) SLEPS potential and (b) MLEPS potential.

600 K shows almost none. Also, around the new resonance at 100 K, we see significant excitation of the spectator atom as was to be expected based on the other resonances.

In Figure 4a, we also plotted the percentage translational energy, H_2 vibrational energy, and spectator vibrational energy for the (2+1)D calculations. It is clear from this figure that only a small percentage of energy will end up in the spectator mode for the SLEPS potential. However, it is also clear that introducing the spectator mode does introduce a redistribution of energy in the reaction. At 100 K, according to Figure 4a we see a flow away from vibrational excitation of the product H_2 molecule. This is corroborated by Figure 7a, in which we plotted the populations of the vibrational levels (ν) for the 2D calculations (sticks) together with the populations of the (ν, ξ) levels of the (2+1)D calculations (histogram). Here, we see a clear decrease in the population for the (2+1)D ($\nu = 3, \xi = 0$) state compared to the 2D ($\nu = 3$) state. This is only marginally compensated by higher populations for the ($\nu = 2$, $\xi = 0$), ($\nu = 1$, $\xi = 0$), and ($\nu = 3$, $\xi = 1$) states, leading to an overall conclusion that for the SLEPS potential at 100 K inclusion of the spectator bond will lead to lower vibrational excitation.

Interesting enough, we also see a change in the vibrational and translational energy percentages, where there is almost no population in excited spectator modes, e.g., between 400 and 600 K. This means that, even if no excited spectator atoms are present after the collision, this bond is still used during the collision as a reservoir which enables energy transfer from one mode to another.

4.2.2. MLEPS Potential. Comparing the reaction probabilities, summed over all spectator states, for the (2+1)D calculations in Figure 5b with the reaction probabilities for the 2D calculations in Figure 3b, we see more differences than in the case of the SLEPS potential. The resonance at 600 K has shifted to lower energies, and we see changes in the reaction probabilities at 800 K. However, most importantly, we see a reversal of the curves for the $\nu = 3$ and $\nu = 4$ states at energies below 150 K.

The differences between the 2D and (2+1)D calculations between 150 and 600 K appear to be small. This is despite the fact that if one looks at the reaction probabilities summed over all H_2 states, one finds a considerable population in the $\xi = 1$ and 2 states of the spectator atom. This happens over a much wider range of energies than in the SLEPS case, where excitation of the spectator modes appeared to be restricted to resonance energies. This has to be caused by the fact that the potential for the spectator atom is much shallower for the MLEPS potential, making the energy differences between states much smaller and subsequently making excitation to higher-lying states easier.

If we look at the (2+1)D reaction probabilities at 97 K and compare those to the 2D reaction probabilities (Figure 7b), we see that the effect of adding the spectator bond is a decrease in the (ν, $\xi = 0$) probabilities. However, for the ($\nu = 2$, ξ) and ($\nu = 3$, ξ) levels, this is compensated by the addition of population in the $\xi = 1$ and 2 levels. As a result, the average vibrational energy in the H_2 molecule does not change significantly in going from the 2D to the (2+1)D calculations. This is clear from Figure 4b. This figure shows that the energy needed

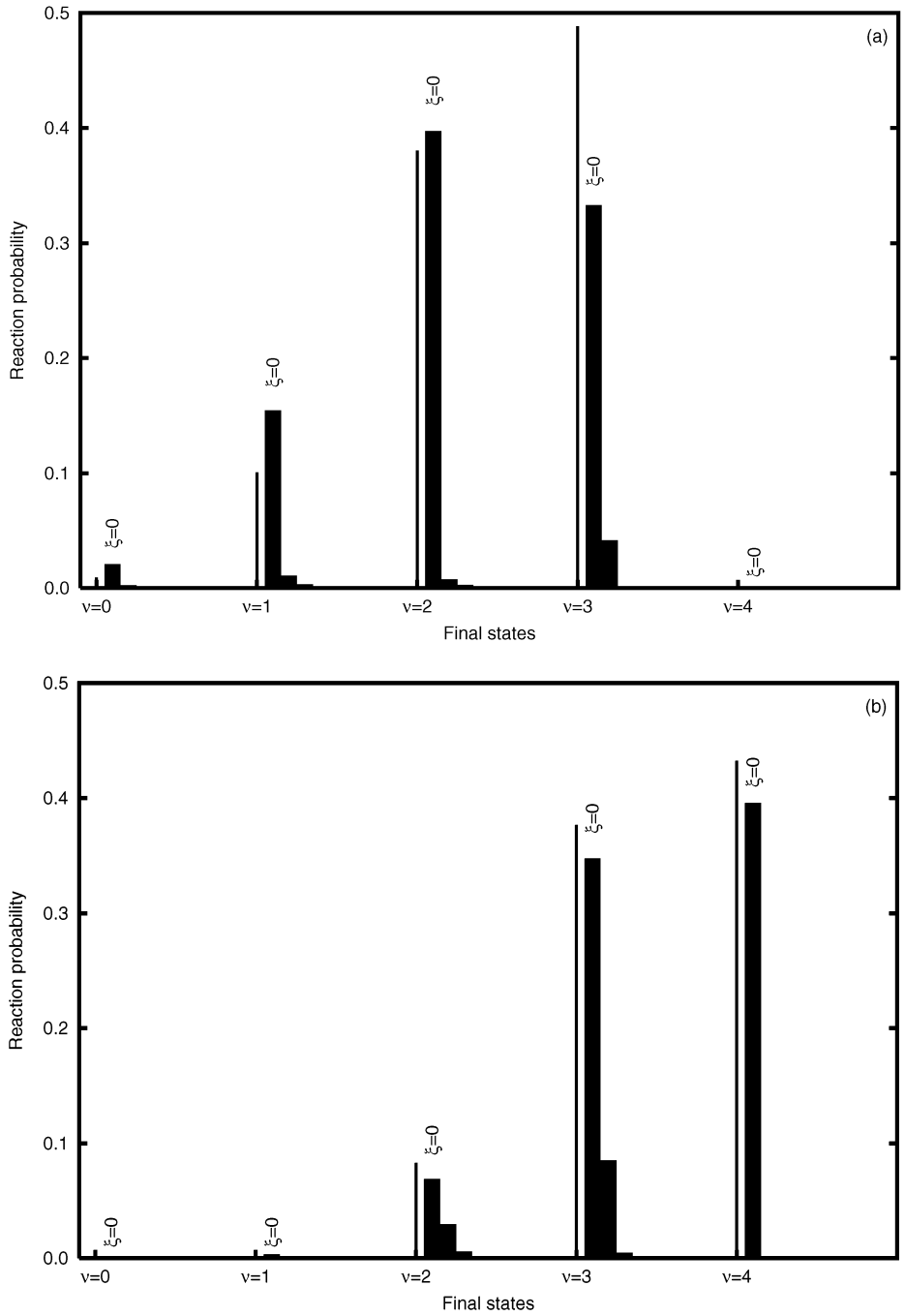

Figure 7. Reaction probabilities for the 2D calculations (stick) and the (2+1)D calculations (boxes): (a) SLEPS potential at 97 K and (b) MLEPS potential at 99 K.

for the excitation of the spectator bond is mainly coming from translational energy for the energy range plotted. Moreover, over most of the energy range, the percentage H_2 vibrational energy increases instead of decreases. The largest changes occur at 600 K, where we also see a large increase in the population of the $\xi = 2$ and 3 levels. Around this energy there is also a small population of the $\xi = 4$ and 5 states, but this is less than 1%. Therefore, these curves were left out to make Figure 7b easier to comprehend. The next largest change occurs at 200 K but is not accompanied by a large change in the population levels of the spectator mode, which means that also here we see that the spectator bond also functions as a reservoir to affect energy redistribution at specific energies, even though no energy ends up in the spectator bond after the collision.

5. Conclusions

In this paper, we investigated the surface catalyzed formation of H_2 on graphite, a model for interstellar dust. In light of recent experimental results[10,11] that show much less vibrational and rotational excitation than previous theoretical work[2,3,15,17−19,21] and in light of recent observations that show no evidence of highly excited H_2, we investigated the influence of the presence of other (nonreactive) H atoms on the surface on the reaction dynamics. This was done by assuming a monolayer of hydrogen, physisorbed on a graphite surface. The influence of the layer was investigated by comparing collinear 2D calculations, in which all nonreactive atoms of the layer are fixed, to (2+1)D calculations, in which also one nonreactive atom is allowed to vibrate.

To perform our calculations, we developed a new model potential which could take into account multiple atoms on a surface. This was done by taking the LEPS formulation[54] used previously[2] and using it as a pair potential for each pair of H atoms. Two different LEPS forms were fitted to points generated using periodic DFT: the standard LEPS form (SLEPS) and the modified LEPS form (MLEPS). We have to point out here that these potentials, like the potentials used before, are highly qualitative and that significant changes in the reaction probabilities can occur if more accurate potentials are used. Our results also show that for this system the precise fit is also important, because the MLEPS and SLEPS reaction probabilities are distinctly different, in particular with regards to the presence and position of resonances. The SLEPS potential show lower overall vibrational excitation, most likely due to the potential, which shows a much narrower entrance channel and interaction region than the MLEPS potential.

The addition of the extra vibrational degree-of-freedom has some effect on both the SLEPS and the MLEPS calculations, in that at low translational energies and at the resonances the maximum H_2 vibrational quantum number is lower in the (2+1)D calculations than in the 2D calculations. Also, at low energies and at the resonances, we find significant excitation of the spectator H-graphite mode. The effect is much more pronounced for the MLEPS potential than for the SLEPS potential, which again is assumed to be due to the much wider entrance channel and interaction region for the MLEPS potential. We also have to point out that the possible effect of the additional vibrating H would be much larger in a calculation in which we would also allow nonzero impact parameters, which obviously more closely resembles the experimental setup.

We have also seen that even when there is no significant excitation of the spectator H atom a significant redistribution of the available energy can take place. This means that the spectator-graphite bond can function as a reservoir of energy during the reaction. This energy can then be released or be retained during the H_2 desorption.

No evidence of highly excited H_2 has been found sofar in the interstellar medium in any of the astronomical observations. Moreover, experiments done on this reaction at University College London show much less vibrational excitation than predicted in any previous theoretical work. Therefore, the main purpose of our calculations has been to investigate the discrepancies between the results from earlier calculations and observational and experimental data in order to be able to ascertain which processes might have been wrongly ignored previously. Via that route, we hoped to further our understanding of this fundamental astrochemical process. Our calculations show that the presence of other light atoms or molecules (such as H_2) would significantly influence the reaction probabilities for the formation of H_2 in the interstellar medium. Therefore, their presence may be a possible explanation for the much lower degree of vibrational excitation found sofar in the experiment and the absence of evidence for highly excited H_2 in the observational studies.[22,73]

Acknowledgment. The research was funded by the Particle Physics and Astronomy Research Council, the Engineering and Physical Sciences Research Council, and the Leverhulme Trust. The authors thank the members of the Centre for Cosmic Chemistry and Physics at University College London for helpful discussions.

References and Notes

(1) Farebrother, A. J.; Meijer, A. J. H. M.; Clary, D. C.; Fisher, A. J. *Chem. Phys. Lett.* **2000**, *319*, 303.
(2) Meijer, A. J. H. M.; Farebrother, A. J.; Clary, D. C.; Fisher, A. J. *J. Phys. Chem. A* **2001**, *105*, 2173.
(3) Meijer, A. J. H. M.; Farebrother, A. J.; Clary, D. C. *J. Phys. Chem. A* **2002**, *106*, 8996.
(4) Gough, S.; Schermann, C.; Pichou, F.; Landau, M.; Cadez, I.; Hall, R. I. *Astron. Astrophys.* **1996**, *305*, 687.
(5) Katz, N.; Furman, I.; Biham, O.; Pirronello, V.; Vidali, G. *Astrophys. J.* **1999**, *522*, 305.
(6) Vidali, G.; Pirronello, V.; Liu, C.; Shen, L. *Astrophys. Lett.* **1998**, *35*, 423.
(7) Pirronello, V.; Biham, O.; Liu, C.; Shen, L.; Vidali, G. *Astrophys. J.* **1997**, *483*, L131.
(8) Pirronello, V.; Liu, C.; Roser, J. E.; Vidali, G. *Astron. Astrophys.* **1999**, *344*, 681.
(9) Biham, O.; Furman, I.; Katz, N.; Pirronello, V.; Vidali, G. *Mon. Not. R. Astron. Soc.* **1998**, *296*, 869.
(10) Perry, J. S. A.; Gingell, J. M.; Newson, K. A.; To, J.; Watanabe, N.; Price, S. D. *Meas. Sci. Technol.* **2002**, *13*, 1414.
(11) Perry, J. S. A.; Price, S. D. *Astrophys. Space Sci.* **2003**, submitted.
(12) Zecho, T.; Güttler, A.; Sha, X.; Lemoine, D.; Jackson, B.; Küppers, J. *Chem. Phys. Lett.* **2002**, *366*, 188.
(13) Zecho, T.; Güttler, A.; Sha, X.; Jackson, B.; Küppers, J. *J. Chem. Phys.* **2002**, *116*, 3063.
(14) Parneix, P.; Bréchignac, P. *Astron. Astrophys.* **1998**, *334*, 363.
(15) Jackson, B.; Lemoine, D. *J. Chem. Phys.* **2001**, *114*, 474.
(16) Sha, X.; Jackson, B. *Surf. Sci.* **2002**, *496*, 318.
(17) Sha, X.; Jackson, B.; Lemoine, D. *J. Chem. Phys.* **2002**, *116*, 7158.
(18) Ree, J.; Kim, Y. H.; Shin, H. K. *Chem. Phys. Lett.* **2002**, *353*, 368.
(19) Rutigliano, M.; Cacciatore, M.; Billing, G. D. *Chem. Phys. Lett.* **2001**, *340*, 13.
(20) Jeloaica, L.; Sidis, V. *Chem. Phys. Lett.* **1999**, *300*, 157.
(21) Morisset, S.; Aguillon, F.; Sizun, M.; Sidis, V. *Phys. Chem. Chem. Phys.* **2003**, *5*, 506.
(22) Tine, S.; Williams, D. A.; Clary, D. C.; Farebrother, A. J.; Fisher, A. J.; Meijer, A. J. H. M.; Rawlings, J. M. C.; Davis, C. J. *Astrophys. Space Sci.* **2003**, in press.
(23) Takahashi, J. *Astrophys. J.* **2001**, *561*, 254.
(24) Takahashi, J. *Astrophys. J.* **2001**, *561*, 843.
(25) Biham, O.; Furman, I.; Pirronello, V.; Vidali, G. *Astrophys. J.* **2001**, *553*, 595.
(26) Ferro, Y.; Marinelli, F.; Allouche, A. *J. Chem. Phys.* **2002**, *116*, 8124.
(27) Ferro, Y.; Marinelli, F.; Allouche, A. *Chem. Phys. Lett.* **2003**, *368*, 609.
(28) Farebrother, A. J. Formation of Diatomic Molecules at Surfaces. Ph.D. Thesis, University College London, London, U.K., 2001.
(29) Masuda, K.; Takahashi, J.; Mukai, T. *Astron. Astrophys.* **1998**, *330*, 773.
(30) Takahashi, J.; Masuda, K.; Nagaoka, M. *Mon. Not. R. Astron. Soc.* **1999**, *306*, 22.
(31) Al-Halabi, A.; Kleyn, A. W.; van Dishoeck, E. F.; Kroes, G. J. *J. Phys. Chem. A* **2002**, *106*, 6515.
(32) Zecho, T.; Güttler, A.; Küppers, J. *Chem. Phys. Lett.* **2003**, *370*, 366.
(33) van der Hulst, H. C. *Rec. Astron. Obs.* **1949**, *XI(II)*.
(34) Gould, R. J.; Salpeter, E. E. *Astrophys. J.* **1963**, *138*, 393.
(35) Hollenbach, D.; Salpeter, E. E. *Astrophys. J.* **1971**, *163*, 155.
(36) Williams, D. A.; Herbst, E. *Surf. Sci.* **2002**, *500*, 823.
(37) Duley, W. W.; Williams, D. A. *Interstellar Chemistry*; Academic Press: London, U.K., 1984.
(38) Mathis, J. S.; Rumpl, W.; Nordsieck, K. H. *Astrophys. J.* **1977**, *217*, 425.
(39) Fitzpatrick, E. L.; Massa, D. *Astrophys. J. Suppl. Ser.* **1990**, *72*, 163.
(40) Li, A. G.; Greenberg, J. M. *Astron. Astrophys.* **1997**, *323*, 566.
(41) Draine, B. T. In *Interstellar Dust*; Allamandola, L. J., Tielens, A. G. G. M., Eds.; Kluwer: Dordrecht, The Netherlands, 1989; p 483, vol. 135 of *IAU Symposium*.
(42) Papoular, R.; Conard, J.; Guillois, O.; Nenner, I.; Reynaud, C.; Rouzaud, J.-N. *Astron. Astrophys.* **1996**, *315*, 222.
(43) Eley, D. D.; Rideal, E. K. *Nature* **1940**, *146*, 401.
(44) Cazaux, S.; Tielens, A. G. G. M. *Astrophys. J.* **2002**, *575*, L29.
(45) Shalashilin, D. V.; Jackson, B.; Persson, M. *Faraday Discuss.* **1998**, *110*, 287.
(46) Shalashilin, D. V.; Jackson, B.; Persson, M. *J. Chem. Phys.* **1999**, *110*, 11038.
(47) Guvenc, Z. B.; Sha, X.; Jackson, B. *J. Phys. Chem. B* **2002**, *106*, 8342.
(48) Guvenc, Z. B.; Sha, X.; Jackson, B. *J. Chem. Phys.* **2001**, *115*, 9018.
(49) Meijer, A. J. H. M.; Fisher, A. J. unpublished results, 2003.
(50) Schwartz, C. *J. Math. Phys.* **1985**, *26*, 411.
(51) Groenenboom, G. C.; Colbert, D. T. *J. Chem. Phys.* **1993**, *99*, 9681.

(52) Note the error with the signs in refs 51 and 53.
(53) Groenenboom, G. C. private communication, 1996.
(54) McCreery, J. H.; Wolken, G., Jr. *J. Chem. Phys.* **1975**, *63*, 2340.
(55) Persson, M.; Strömqvist, J.; Bengtsson, L.; Jackson, B.; Shalashilin, D. V.; Hammer, B. *J. Chem. Phys.* **1999**, *110*, 2240.
(56) Gray, S. K.; Balint-Kurti, G. G. *J. Chem. Phys.* **1998**, *108*, 950.
(57) Meijer, A. J. H. M.; Goldfield, E. M.; Gray, S.; Balint-Kurti, G. G. *Chem. Phys. Lett.* **1998**, *293*, 270.
(58) Balint-Kurti, G. G.; Gonzales, A. I.; Gray, S. K.; Goldfield, E. M. *J. Chem. Soc., Faraday Discuss.* **1998**, *110*, 169.
(59) Gray, S. K.; Goldfield, E. M.; Schatz, G. C.; Balint-Kurti, G. G. *Phys. Chem. Chem. Phys.* **1999**, *1*, 1141.
(60) Gray, S. K.; Wozny, C. E. *J. Chem. Phys.* **1989**, *91*, 7671.
(61) Zhang, D. H.; Zhang, J. Z. H. *J. Chem. Phys.* **1994**, *101*, 3671.
(62) Meijer, A. J. H. M.; Goldfield, E. M. *J. Chem. Phys.* **1998**, *108*, 5404.
(63) Zhang, J. Z. H. *Theory and Application of Quantum Molecular Dynamics*; World Scientific: Singapore, 1999.
(64) Wang, Y.; Perdew, J. P. *Phys. Rev. B* **1991**, *44*, 13298.
(65) Kresse, G.; Hafner, J. *Phys. Rev. B* **1993**, *47*, 558.
(66) Kresse, G.; Hafner, J. *Phys. Rev. B* **1994**, *49*, 14251.
(67) Kresse, G.; Furthmuller, J. *Phys. Rev. B* **1996**, *54*, 11169.
(68) Kresse, G.; Furthmuller, J. *Comput. Mater. Sci.* **1996**, *6*, 15.
(69) Dabrowski, I. *Can. J. Phys.* **1984**, *62*, 1639.
(70) Abgrall, H.; Roueff, E.; Launay, F.; Roncin, J.; Subtil, J. *J. Mol. Spectrosc.* **1993**, *157*, 512.
(71) *The NAG Fortran library, Mark 18*; The Numerical Algorithms Group Limited: Oxford, U.K., 1998.
(72) Meijer, A. J. H. M. *Comput. Phys. Commun.* **2001**, *141*, 330.
(73) Takahashi, J. unpublished results, 2003.